The role of beach morphology on coastal cliff erosion under extreme waves

Claire Earlie,[1]* (iD) Gerhard Masselink[2] and Paul Russell[2]
[1] School of Earth and Ocean Science, Cardiff University, Cardiff, UK
[2] Marine Science and Engineering, University of Plymouth, Plymouth, UK

*Correspondence to: Claire Earlie, School of Earth and Ocean Science, Cardiff University, Room 1.32, Main Building, Park Place, Cardiff, South Glamorgan, CF10 3AT, UK.E-mail: earliec@cardiff.ac.uk

ESPL

Earth Surface Processes and Landforms

ABSTRACT: Erosion of hard-rock coastal cliffs is understood to be caused by a combination of both marine and sub-aerial processes. Beach morphology, tidal elevation and significant wave heights, especially under extreme storm conditions, can lead to variability in wave energy flux to the cliff-toe. Wave and water level measurements in the nearshore under energetic conditions are difficult to obtain and *in situ* observations are rare. Here we use monthly cliff-face volume changes detected using terrestrial laser scanning alongside beach morphological changes and modelled nearshore hydrodynamics to examine how exposed cliffs respond to changes in extreme wave conditions and beach morphology. The measurements cover the North Atlantic storms of 2013 to 2014 and consider two exposed stretches of coastline (Porthleven and Godrevy, UK) with contrasting beach morphology fronting the cliffs; a flat dissipative sandy beach at Godrevy and a steep reflective gravel beach at Porthleven. Beach slope and the elevation of the beach–cliff junction were found to influence the frequency of cliff inundation and the power of wave–cliff impacts. Numerical modelling (XBeach-G) showed that under highly energetic wave conditions, i.e. those that occurred in the North Atlantic during winter 2013–2014, with $H_s = 5.5$ m (dissipative site) and 8 m (reflective site), the combination of greater wave height and steeper beach at the reflective site led to amplified wave run-up, subjecting these cliffs to waves over four times as powerful as those impacting the cliffs at the dissipative site (39 kWm^{-1} compared with 9 kWm^{-1}). This study highlighted the sensitivity of cliff erosion to extreme wave conditions, where the majority (over 90% of the annual value) of cliff-face erosion ensued during the winter. The significance of these short-term erosion rates in the context of long-term retreat illustrates the importance of incorporating short-term beach and wave dynamics into geomorphological studies of coastal cliff change. © 2017 The Authors. Earth Surface Processes and Landforms published by John Wiley & Sons Ltd.

KEYWORDS: cliff erosion; terrestrial laser scanning; XBeach-G; beach morphology; extreme waves

Introduction

Coastal cliff erosion is understood to be due to a complex combination of sub-aerial and marine processes weakening the structural integrity of the cliffs, leading to gradual erosion and episodic mass failure (Pethick, 1984; Trenhaile, 1987; Sunamura, 1992). The variety of cliff profiles and cliff types around the world indicates that there are a wide range of processes involved in shaping cliffed coasts (Emery and Kuhn, 1982). These processes may include erosion due to wave-attack via abrasion, attrition, quarrying and hydraulic action, or physical and chemical weathering of cliff material as a result of rainfall, changes in temperature, biochemical and biophysical erosion (Trenhaile, 1987, 2005, 2016; Sunamura, 1992; Masselink and Hughes, 2003). The mechanisms of cliff failure and conditions leading to the erosion of cliffs have therefore been the topic of investigation for many decades.

Many cliff erosion and rocky coast geomorphological studies have considered the role of beach morphology (width, height and volume) in modifying the dissipation of wave energy and the extent of cliff-toe/shore platform protection from erosion (Trenhaile, 1987, 2016; Sunamura, 1992). Modelling the erosion of cohesive clay cliffs related to shore platform development, Trenhaile (2005, 2009) has shown that nearshore shore platform profile gradient and beach sediment thickness controlled the extent of cliff erosion due to the proximity of breaking waves to the cliff face, where waves break close to the cliff on steeply sloping profiles and farther offshore on wider, more gently sloping profiles. The presence of a shore platform beneath a thin veneer of sand is thought to potentially provide protection to cliffs (Trenhaile, 2016). Other studies have also found sediment budget to be an important factor in terms of cliff erosion, due to longshore sediment transport contributing to beach width fronting the cliffs (Sunamura, 1976, 1992; Dickson *et al.*, 2007; Carpenter *et al.*, 2014; Trenhaile, 2016) and also beach presence/absence itself and the thickness of the beach playing a role in the abrasion/protection of cliffed coasts (Limber and Murray, 2011; Trenhaile, 2016). In terms of cliff response to sea level rise, it is typically understood that a decrease in beach volume or elevation fronting a cliff will lead to an increase in cliff erosion (Walkden and Hall, 2005, 2011; Young and Ashford, 2006; Lee, 2008; Walkden and Dickson, 2008).

In order to understand the relationship between the assailing forces and cliff failure mechanisms, an accurate quantification is also needed of nearshore wave energy and water levels, as well as the morphology of the beach and meteorological conditions (Ruggerio *et al.*, 2001, 2004; Trenhaile, 2005, 2016). Studies have previously related the interplay between wave run-up, offshore wave climate and beach levels using models (Shih *et al.*, 1994; Ruggerio *et al.*, 1996; Trenhaile, 2005; Lee, 2008; Walkden and Dickson, 2008; Young *et al.*, 2013, 2014); yet, few studies use *in situ* observations, and those that do tend to use proxies or assumptions for beach morphological, wave and water level parameters (Trenhaile, 2009; Lim *et al.*, 2011; Norman, 2012). In terms of field measurements, studies using airborne LiDAR (light detection and ranging) data found that soft-rock sea-cliff erosion along the California coast was strongly related to the effective beach width, elevation of the beach at the cliff-toe and horizontal run-up excursion (Ruggerio *et al.*, 2001; Sallenger *et al.*, 2002).

In situ measurements of seismically detected cliff-top ground motions have proved to be a viable proxy for cliff-base wave conditions (Norman *et al.*, 2013; Young *et al.*, 2011, 2012, 2013, 2016). An experiment at the same site used in this study (Porthleven; Earlie *et al.*, 2015) coupled wave–cliff impacts from a camera and wave energy from an offshore wave buoy with seismically detected cliff top-ground motions. Cliff-base sand and water levels along the southern California coastline, with concurrent monitoring of cliff-top ground motion (Young *et al.*, 2016) found similar results, where cliff-top ground response was controlled by tide, incident waves and, in addition, beach sand levels. The importance of water levels on cliff erosion was also highlighted by Vann Jones *et al.* (2015), who found that rock falls from the entire cliff-face, are a result of marine processes and result in failure extending the full height of the cliff, not just the cliff-toe. In addition to this, cliff-toe inundation duration was not found to be responsible for increased rock fall activity; however, the wave energy expended on the cliffs during these inundation periods was not considered in Vann Jones' study, and the relationship between the failure and forcing proved to be more complex.

Terrestrial laser scanning (TLS) is a common method for investigating short-term (monthly) cliff dynamics due to its high-resolution data capture and suitability for rapid deployment in the field. Over the last decade, TLS has been adopted for monitoring both hard- and soft-rock cliffs to obtain an accurate three-dimensional (3D) surface of a cliff-face (Rosser *et al.*, 2005, 2007; Poulton *et al.*, 2006; Abellan *et al.*, 2011; Dewez *et al.*, 2013; Rohmer and Dewez, 2013). These surveys may provide insight into where and when failures are occurring (Rosser *et al.*, 2005, 2007; Norman, 2012; Kuhn and Prufer, 2014; Travelletti *et al.*, 2014), and frequent surveys provide a chronology of material failure relative to the forcing conditions (Lim *et al.*, 2011). Although TLS is a commonly adopted method of measuring coastal morphological change (Rosser *et al.*, 2005, 2007; Abellan *et al.*, 2010; Lague *et al.*, 2013; Travelletti *et al.*, 2014; Vann Jones *et al.*, 2015), few studies compare cliff erosion volumes and locations directly with the nearshore hydrodynamics and beach morphology (Earlie, 2015).

This relationship between the beach and the cliffs has, in the context of climate change and the impacts of sea level rise, been evaluated and modelled on long-term timescales (O(1–2) years) and over large stretches of coast (O(1–2) km) (Walkden and Hall, 2005, 2011; Young and Ashford, 2006). With the exception of Young *et al.* (2016), field measurements of beach morphological changes on the short-term timescale (days to months) are not typically considered in cliff erosion studies. The short-term variability of beach elevation in relation to the cliff-toe and the variety of protection afforded by different beach types (i.e. reflective versus dissipative) is neither compared nor accounted for in many cliff erosion models, and has only recently been investigated in the field (Earlie, 2015). Likewise, studies capturing energetic storm conditions ($H_s > 5$ m) are rare and such extreme, higher energy scenarios have not yet been incorporated into cliff erosion models.

To consider the more imminent risks to infrastructure on particularly vulnerable and eroding stretches of coastline, with dynamics on a much smaller time and spatial scale (months to years; tens of metres), an *in situ* method that is able to quantify change at a higher temporal (monthly or weekly) and spatial scale (centimetres to metres) is required. Annual monitoring of cliff morphology is not suitable for investigating intra-annual dynamics related to, for example, wave height and rainfall variability. With the potential for increased storminess and sea level rise in the future (Cowell *et al.*, 2006; Barros *et al.*, 2014; Haigh *et al.*, 2016), this begs the question of 'how will the cliffs stand up to more extreme and frequent assailing forces?'

This study aims to help fill the gaps that currently exist in our understanding of the processes leading to cliff erosion. Here we consider the processes that govern short-term cliff dynamics more specifically, i.e. waves, rainfall, water levels, beach morphology, as it is the integration of these short-term cliff dynamics that determine long-term cliff recession. Using *in situ* monitoring at a high spatial and temporal resolution, complemented by numerical modelling, we will examine the role of beach morphology in controlling delivery of wave energy, and in particular extreme wave energy, to the cliffs.

Study Area

Two vulnerable coastal cliff sites on the southwest peninsula of the UK, one facing west (Godrevy, north Cornwall) and the other facing southwest (Porthleven, south Cornwall) (Figure 1), were selected for this study. Both sites experience a highly energetic wave climate, are exposed to both locally-generated wind waves and Atlantic swell from the west (Scott *et al.*, 2011), and are subjected to a macro-tidal regime. The two sites have similar geology (lithology, rock mass characteristics) and morphology (cliff height), but differ in their coastal setting (shoreline orientation, wave exposure) and the morphology of the beach in front of the cliff (beach gradient, bathymetry, elevation of beach–cliff intersection). The key characteristics of both sites are summarized in Table I. Along with many other cliff locations along the southwest coast of England, the two sites experience current management issues due to on-going cliff instability impacting on infrastructure, thereby posing risks to beach and coast path users.

Godrevy

Godrevy is situated on the southwest peninsula along the west-facing coast of Cornwall. Exposed to an energetic wave climate, the cliffs are subject to both north-westerly and westerly Atlantic swell. The tidal regime at Godrevy is macro-tidal with a mean spring range of 5.9 m. The cliffs are fronted by a gently sloping beach ($\tan\beta = 0.02$) composed of well-sorted medium sand ($D_{50} = 0.25$–0.5 mm) with a very narrow (< 10 m wide), slightly steeper upper beach composed of mixed sand and gravel/pebbles ($D_{50} = 16$–30 mm) (Scott, 2012). The coastal slope offshore of Godrevy is very wide and flat, with the 10-m contour about 1.5 km offshore. The seabed then slopes gently out to the 20-m contour which lies at about 2.5 km offshore to the west-northwest [Lee, 2002; Channel Coastal Observatory (CCO), 2015].

The cliffs rise 8–15 m above the beach and the beach elevation at the cliff-toe varies seasonally between 2.5 and 4.7 m (in
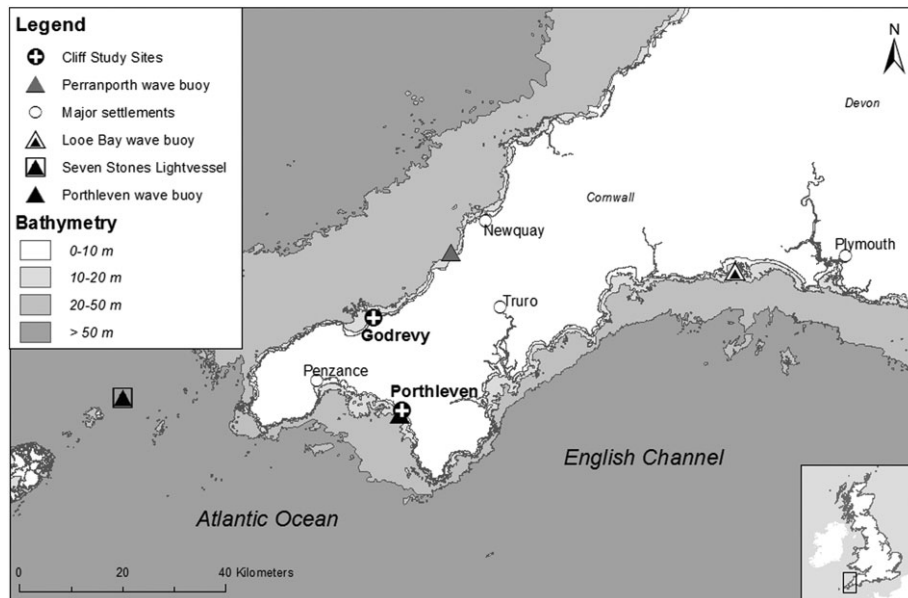
Figure 1. Location of study sites, wave buoys and tide gauges. The line separating the light and dark grey zones represents the 50-m Chart Datum (CD) contour line.

Table I. Summary of physical characteristics at each site. Cliff heights and beach–cliff junction (b–c junction) elevation and are shown in metres above Ordnance Datum Newlyn (m ODN)

Site characteristic	Godrevy	Porthleven
Cliff height (above beach)	8–15 m	8–12 m
Length of cliff	~300 m	~300 m
Lithological units	Devonian sandstones and mudstones (2–15 m) overlain by Quaternary head deposit (~2 m)	Mylor slates (5–10 m) overlain by Quaternary head deposit (2–4 m)
b–c junction (annual range)	2.5–4.7 m	4.4–7 m
Beach slope ($\tan\beta$)	0.02 (s.d. 0.005)	0.17 (s.d. 0.03)
Offshore slope	0.002–0.01	0.008–0.01
Mean Spring Tidal range	5.9 m	4.7 m
Mean high water springs (MHWS)	3.2 m (6.6 m CD)	2.5 m (5.5 m CD)
Winter H_s (October–March)	1.7 m (mean) 5.6 m (max)	1.4 m (mean) 10.3 m (max)
Summer H_s (Apr–September)	0.8 m (mean) 3.6 m (max)	0.7 m (mean) 3.8 m (max)
Winter T_p (October–March)	12 seconds (mean) 22 seconds (max)	9 seconds (mean) 28 seconds (max)
Summer T_p (April–September)	9 seconds (mean) 20 seconds (max)	7 seconds (mean) 22 seconds (max)

Note: Tidal elevations are presented in metres relative to ODN and Chart Datum (m CD). Seasonal means for 2013–2014 for significant wave height (H_s) and peak wave period (T_p) are taken from the Channel Coastal Observatory (CCO) directional wave rider wave buoy (CCO, 2015).

m Ordnance Datum Newlyn, ODN, which is *c.* 0.2 m above mean sea level, MSL) (Table I). The geological units at Godrevy consist of an underlying, more resistant basal layer of weakly metamorphosed sandstones and mudstones overlain by superficial head deposits, varying in thickness along the cliffs. The boundary between the two major units rises from beach level at the northern end of the embayment to an elevation of about 15 m at the southern end (Figure 2). The basal layer (Porthtowan formation) comprises weakly metamorphosed Upper Devonian sandstones and mudstones (Shail *et al.*, 1998). A unit of superficial head deposit overlying the basal layer is composed of a poorly sorted mixture of variably sized fragments in a silty cohesive matrix overlain by a layer of wind-blown sand (Shail and Coggan, 2010).

Porthleven

The study site at Porthleven (Figure 1) is situated along a 300-m stretch of uninhabited cliffed coastline just southeast of Porthleven along the south-facing coast of Cornwall, exposed to south-westerly Atlantic swell. The tidal regime is macro-tidal

with a mean spring range of 4.7 m. The cliffs rise 8–12 m above a steep ($\tan\beta = 0.17$), fine-gravel ($D_{50} = 2–8$ mm) beach (Poate *et al.*, 2009), and the beach elevation at the cliff-toe varies seasonally between 4.4 m ODN after storms in the winter and 7 m ODN after prolonged calm conditions during summer. The coastal slope at Porthleven is slightly steeper than at Godrevy, with the 10-m contour about 600 m offshore and the 20-m contour about 1.5 km offshore (Lee, 2002; CCO, 2015) (Table I).

The cliffs are mainly formed of Late Devonian Mylor slate lithofacies, comprising pale grey-green mudstone with interbedded-siltstone and fine-grained sandstone (Leveridge and Shail, 2011) (Figure 3). These cliffs are bounded at either end of the bay by Porthscatho lithofacies of alternating beds of green-grey sandstone and dark-grey mudstone (Leveridge and Shail, 2011). Much like the cliffs at Godrevy, this basal layer also displays evidence of complex deformation during the late Carboniferous tectonic evolution of the southwest of the UK (Alexander and Shail, 1996; Shail and Coggan, 2010). The cliffs are cut by a variably reactivated network of late Carboniferous–Triassic fractures, joints and faults. Along with the relative resistance of the rocks, it is the orientation, spacing, roughness
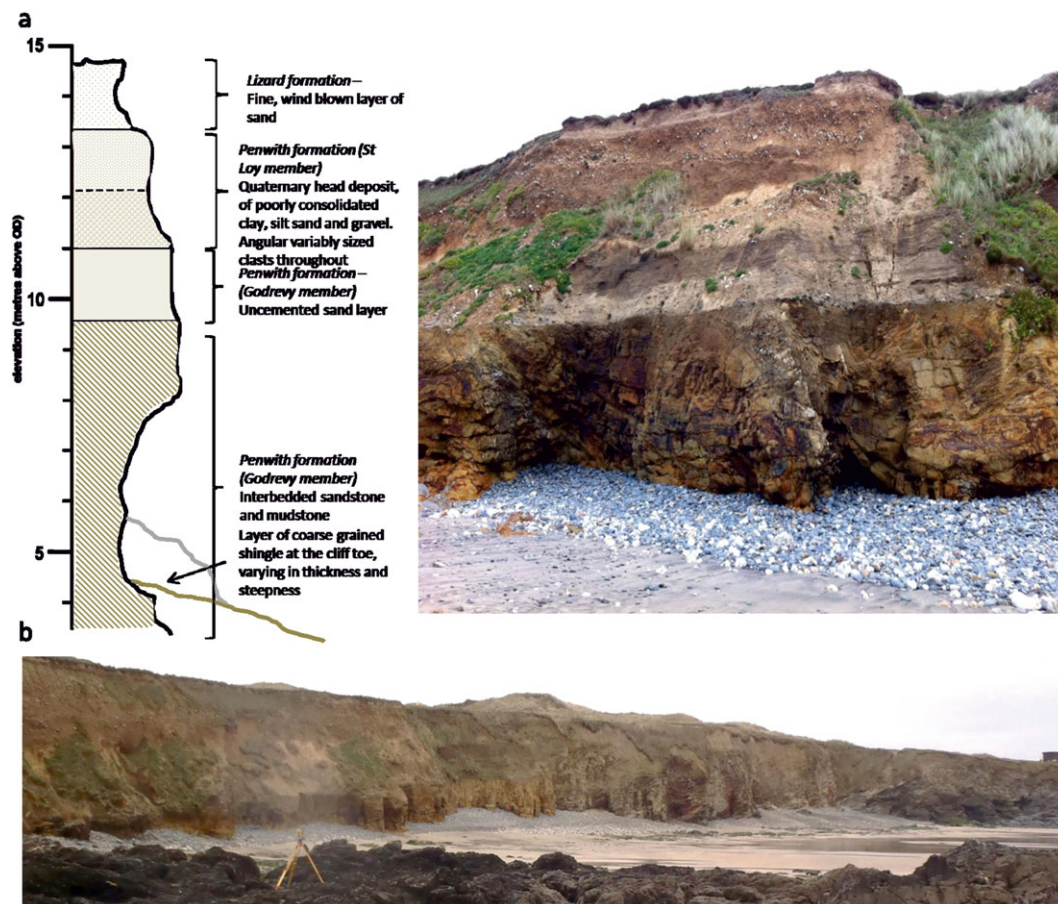
Figure 2. (a) Sketch and photograph of a profile through a section of cliff at Godrevy summarizing the succession of basal layer and superficial units; (b) 300-m wide panoramic perspective of the cliff frontage and beach. [Colour figure can be viewed at wileyonlinelibrary.com]
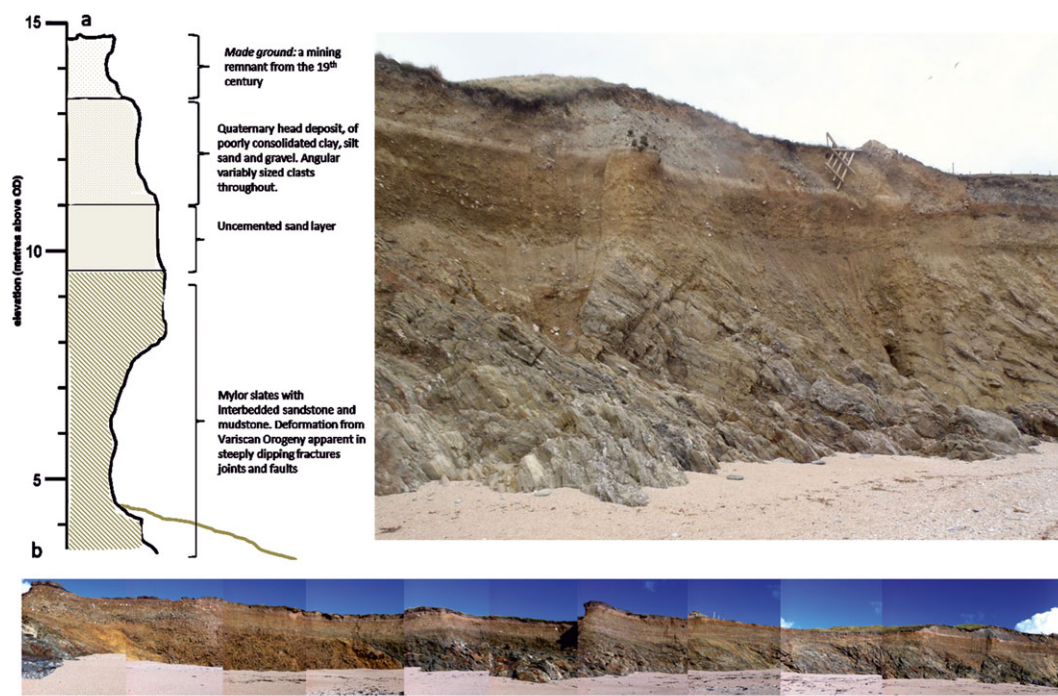

Figure 3. (a) Sketch and photograph of a profile through a section of cliff at Porthleven summarizing the stratigraphic sequence of basal layer and superficial units; (b) 300-m wide panoramic perspective of the cliff frontage and the beach. [Colour figure can be viewed at wileyonlinelibrary.com]

and frequency of these features that ultimately dictate the likelihood and mode of failure (Wyllie and Mah, 2004). The Mylor slates are overlain by a 2–4 m thick Quaternary head deposit of poorly-consolidated clay, silt, sand and gravel capped with a thin layer of 'made ground' (0.5–1.5 m); a remnant of mining activity in the late nineteenth century (Bird, 1998).

Method

Site set-up

The same experimental set-up was adopted at both locations for a survey period of one year, from 10 July 2013 to 17 July 2014. Inshore waves and nearshore water levels were measured using directional wave buoys, tide gauges and local pressure transducers. The cliffs and beaches were surveyed monthly during spring low tide and in response to extreme storms, when conditions permitted.

Wave climate and water levels

Inshore wave climate

Inshore wave statistics (significant wave height H_s, peak wave period T_p and wave direction θ were obtained from directional Waverider wave buoys. For Porthleven, the wave buoy located directly offshore in 14 m water depth was used; for Godrevy, the wave buoy at Perranporth located 20 km to the north of Godrevy in 15 m water depth was used (Figure 1; Table I). During the extreme energetic wave conditions over February 2014, both wave buoys malfunctioned, causing a 34-day data gap between 8 February and 12 March at Godrevy, and a 28-day gap between 4 February and 5 March at Porthleven.

To address the gap in the Porthleven wave record, the wave buoy located at Looe Bay 70 km to the east (Figure 1) was used. Over a three-year (2011–2014) period, H_s at Looe Bay (under southerly and south-westerly swell directions; 180°–240°) was 5% smaller than that at Porthleven. During the 28-day period of missing data at Porthleven, 87% of the waves originated from this quadrant with a mean θ of 200°. The H_s values for Looe Bay were increased by 5% for this 28-day period and were used to represent the nearshore wave climate at Porthleven over the period of missing data.

There is no wave buoy in the vicinity of Godrevy and therefore the Perranporth wave buoy was used instead (Figure 1). However, the Perranporth wave climate is not directly representative for Godrevy, and there is also a 34-day gap in the wave data corresponding to the most energetic period. To overcome both shortcomings, modelled wave data from a regional SWAN model developed by Austin (2012), which was operational during 2011 and 2012, was used. The model is forced by initial wind and wave output from the National Oceanic and Atmospheric Administration (NOAA) Wave Watch III Global wave model, providing half-hourly statistics of H_s and T_p from a two-dimensional (2D) spectra at a number of output nodes around the coastline, including Perranporth and Gwithian (2 km from Godrevy). The measured and modelled wave data sets were compared for the 2011–2012 period to assess the suitability of using the Perranporth wave buoy (and SWAN data) to represent the inshore wave conditions at Godrevy. For this period, H_s values from westerly and west-north-westerly swell directions (270° and 325°) (the dominant swell direction: 98% of the time at Gwithian) were found to be 26% bigger at Perranporth than those at Gwithian (R^2 = 0.93). The combined Perranporth wave buoy and SWAN data wave record (filling the 34-day data gap) were therefore reduced by 26% to represent nearshore wave conditions at Godrevy.

The inshore data for both sites [combination of Porthleven and (adjusted) Looe Bay wave buoy data for Porthleven; and combination of Perranporth and SWAN modelled Perranporth

data for Godrevy (both adjusted)] were de-shoaled to 25 m depth according to linear wave theory (Komar, 1998) to obtain representative offshore wave conditions.

Tidal levels

Measured water levels (including surge) were obtained from the nearest National Tidal and Sea Level Facility (NTSLF, 2014) tide gauge: the Newlyn tide gauge (20 km distant) for Porthleven and the Ilfracombe tide gauge (130 km distant) for Godrevy (NTSLF, 2014) (Figure 1). Nearshore pressure sensors deployed at both sites only captured mid to high-tide water levels and were either dry or exposed to bores and broken waves in the swash zone at lower tidal elevations. To obtain a full tidal record without the effects of breaking waves, bores and wave set-up, mean half-hourly water levels for a 2-hour period either side of high tide from the locally-deployed pressure sensors were compared with data from the NTSLF tide gauges (NTSLF, 2014) and the tide gauge data were adjusted accordingly to derive a full local tidal record at each site.

Beach morphology

Monthly beach surveys at both sites were conducted using a real time kinematic and differential global positioning system (RTK dGPS). At both sites, a 300-m along-shore section of beach was surveyed from the toe of the cliff to the shoreline using cross-shore transects at 50-m spacing. The cross-shore profiles were used to determine the average slope of the beach and the elevations of the beach–cliff intersection for each month.

Cliff volume loss

Point cloud data acquisition

Both sites were surveyed using a Leica ScanStation 2 Terrestrial Laser Scanner (Leica, 2015) for the first five months of the survey period (July 2013–November 2013) and a Leica P20 for the following eight months (December 2013–July 2014). Both are time-of-flight laser scanners and provide high-resolution long-range point cloud data. A similar set-up was adopted for all monthly scans at both sites and point clouds of the cliff-face were obtained at 2-cm resolution at a 40-m range. To acquire optimum coverage of the cliff-face and minimize occlusion effects due to shadowing/blinding of complex surfaces, the scanner was repositioned 4–5 times along the 300-m cliff frontage.

Point cloud data processing

The geo-referenced registered point clouds were removed of any noise (i.e. birds, people, dogs and cliff-top vegetation) manually and exported as .xyz files for further analysis. The first step in performing point cloud difference analysis is typically to create a mesh of the point cloud surface (Rosser et al., 2005; Dewez et al., 2013). In complex surfaces such as rocky cliff-faces, meshing becomes inaccurate due to the errors involved in interpolating across regions that may show occlusion or the complications associated with overhanging parts of the cliff (Lague et al., 2013). In addition to this, unless the different surveys are carried out from the exact same location and elevation, there is often overestimation of volume change associated with mesh comparisons. This is due to the surface roughness creating differences in occlusion patterns as a result of varying scanner position during different survey periods.

Point cloud data comparison: the M3C2 algorithm
Multiscale Model to Model Cloud Comparison (M3C2) is an algorithm developed to overcome issues associated with comparing complex surfaces and compute accurate point-to-point cloud distances (Lague *et al.*, 2013). It uses surface normal estimations along the 3D surface, with orientations varying according to the surface roughness, and computes the distances between two point clouds along these normal directions. Eliminating the need for surface meshing, the software reduces computation time and retains the high-resolution detail of the cliff-face. Each point cloud distance (between the averages of a number of points within a given area) is provided along with a confidence interval, which is related to the surface roughness and the point cloud registration error (Lague *et al.*, 2013). Surface volume change can then be integrated over the area per point-to-point distance calculation. A more detailed description of the algorithm and a discussion on the validity of the method compared with meshing techniques is provided by Brodu and Lague (2012) and Lague *et al.* (2013).

Directly comparing point-to-point cloud, as opposed to meshing across occluded regions, makes volume calculations more robust as the algorithm is only able to compare two surfaces where data are present. Regions of the cliff-face exhibiting apparent *accretion* as a result of vegetation growth at the top of the cliff-face were excluded from erosion volumes and only negative changes were considered. Accumulation of talus at the toe of the cliff is also excluded by only considering negative changes, therefore only quantifying losses to the cliff system.

Meteorological conditions

Meteorological controls on cliff erosion are typically a function of ground temperatures where repetitive freezing/warming can lead to instability of the soil (Duperret *et al.*, 2005) and precipitation results in an increase in pore water pressure (Sunamura, 1992). In southwest England, temperatures very rarely fall below freezing at the coastline (< five days a year) (Met Office, 2012); therefore, the variability of air/ground temperature is not considered here. Cornwall is, however, one of the wettest regions in the country with rainfall totals of 1000–1500 mm yr^{-1} (Met Office, 2012). Monthly rainfall totals were obtained from nearby weather stations; Camborne (7 km from Godrevy) and Culdrose (3 km from Porthleven) as a proxy for ground saturation (and hence cliff instability) due to rainfall.

Numerical modelling

To complement and help interpret the field observations, the numerical model XBeach-G (McCall *et al.*, 2014) was used to quantify the delivery of wave energy to the base of the cliff under different wave and water level conditions and for different beach levels. XBeach-G is a 1DH (vertically-averaged) processed-based numerical model for predicting storm impacts to gravel beaches, but can also be used for sandy beaches provided the appropriate sediment properties are defined. The model is (wave) phase-resolving and calculates the nearshore and swash hydrodynamics across the beach profile, including interactions with the groundwater table, and, if chosen, also computes sediment transport and morphological change.

XBeach-G is applied to both studied beaches (Godrevy and Porthleven) and is forced with a selection of wave and tide conditions to specifically quantify wave energy at the beach–cliff junction for a one-hour period. The characteristic profile for each beach was taken from the mean profile over the year, measured using dGPS. The profiles were extended offshore to

a depth of 25 m (2.5 km from the shoreline at Godrevy and 1.5 km from the shoreline at Porthleven; UK Hydrographic Office (UKHO), 2016. Details of waves and water levels used in the model are presented later in the paper, based on the waves and water levels measured during the monitoring period.

In addition to the hydrodynamic forcing and the beach gradient (tanβ = 0.02 for Godrevy; tanβ = 0.17 for Porthleven), which collectively control the wave run-up (Shih *et al.*, 1994; Stockdon *et al.*, 2006), another critical factor is the elevation of the beach–cliff junction (hereafter termed b–c junction), and this factor will be varied between runs as well. For both sites, this elevation is always higher than the MSL; in other words, the base of the cliff is either dry (on lower tides) or subjected to swash action (on higher tides). The purpose of the modelling is to quantify the wave energy arriving at the base of the cliff using the modelled time series of water surface elevation η_t and cross-shore current velocity u_t at the b–c junction.

Two parameterizations have been used to quantify the delivery of wave energy to the cliff for the different sites and under different forcing scenarios, with both parameterizations yielding the average energy flux (in kW m^{-1} or kJ s^{-1} m^{-1}) that reaches the b–c junction during the one-hour model run. The nearshore wave energy flux (wave power, P) is typically calculated using linear wave theory as the product of wave energy density E (both potential and kinetic energy contributions) and the celerity of the wave groups Cn. Although this approach is not normally used in the swash zone it serves here to give a first approximation in this case. The modelled run of η_t at the beach–cliff interface and the shallow water approximation of the wave group speed is used to compute:

$$P_{\text{linear}} = ECn = \frac{1}{16}\rho g H_s^2 \sqrt{gh} \tag{1}$$

where ρ is density of seawater, g is gravitational acceleration, H_s is significant wave height estimated from four times the standard deviation (s.d.) of η_t and h is the mean of η_t. In the swash zone, the beach is intermittently wet and dry. The variables H_s and h are only calculated for when $\eta_t > 0$; therefore, the value for P_{linear} represents the average potential wave power for when the beach is inundated (in W m^{-1} or J s^{-1} m^{-1}). The second approximation of the wave energy arriving at the cliff base is based on the kinetic energy P_{kinetic} associated with the swash velocity time series u_t. Using only the onshore velocity component, the (onshore-directed) kinetic energy arriving at the base of the cliff can be computed by averaging over the full one-hour model run to obtain P_{kinetic}

$$P_{\text{kinetic}} = \frac{1}{2}\rho u_t^3 \eta_t \tag{2}$$

Results

Wave climate and water levels

The wave climate at both sites was highly variable over the year, with inshore H_s values ranging from 0.5 m to > 5 m and peak wave periods of 5 to 22 seconds along both the north and the south coast. Spring/summer/autumn wave conditions (July 2013–November 2013 and April 2014–July 2014) were much calmer than the rest of the year with H_s values and T_p values less than 3–4 m and 12 seconds, respectively, whereas from December 2013 to March 2014 wave heights and peak periods ranged from 4 m to > 5 m along the north coast and 4 m to > 10 m along the south coast with wave periods from 15 to 22 seconds.

Average monthly wave conditions at Porthleven [H_s = 1.1 m (s.d. = 0.5 m); T_p = 9 seconds (s.d. = 3 seconds)] were slightly
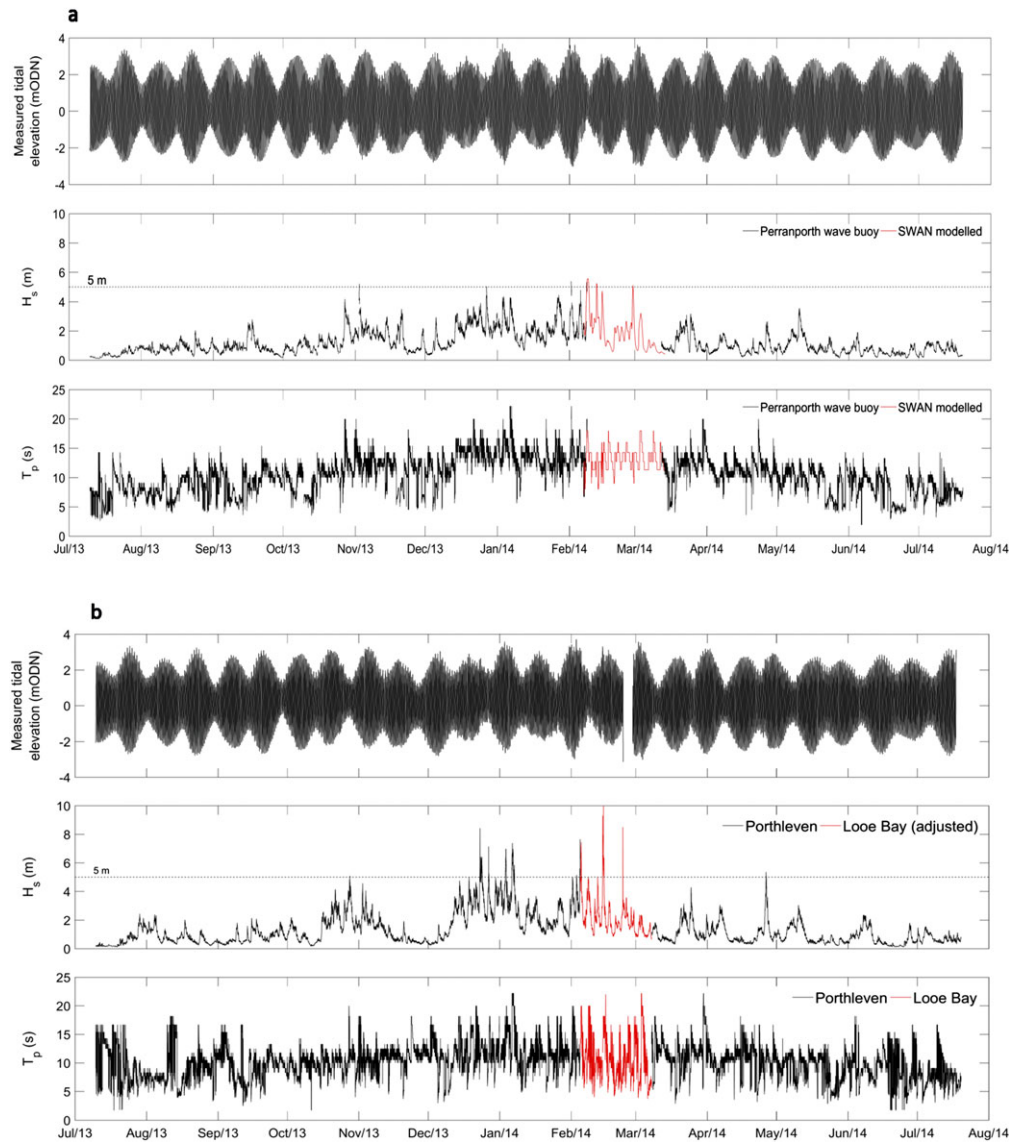
Figure 4. Wave and water level data for (a) Godrevy and (b) Porthleven from July 2013 to July 2014. [Colour figure can be viewed at wileyonlinelibrary.com]

lower over the year than at Godrevy [H_s = 1.3 m (s.d. = 0.6 m); T_p = 11 seconds (s.d. = 2 seconds)]. Significant wave heights reached their maximum in February 2014 at both sites with H_s of 5.6 m and T_p of 15 seconds at Godrevy, and 10.3 m and T_p of 22 seconds at Porthleven. The winter of 2013 to 2014 was the most energetic period the region has experienced since 1948 (Masselink *et al.*, 2016) with inshore H_s values exceeding 5 m and T_p values greater than 15 seconds on seven occasions at Godrevy and nine at Porthleven (Figure 4) from December 2013 to March 2014. As well as considerably high maximum H_s values, conditions were consistently energetic with a 5% exceedance H_s of 8 m and an average T_p of 17 seconds at Porthleven and 5.5 m and 15 seconds at Godrevy.

At both sites, the highest measured tides, as well as H_s values, occurred during the winter (December 2013–March 2014). Tidal elevations, storm durations, associated peak storm surge level and the maximum half-hourly H_s for the individual storms indicate that Porthleven was characterized by more extreme wave conditions during the winter months (Table II). The coincidence of the peak of a storm with a spring high tide, in particular, will result in more wave energy delivered to the cliff. At Porthleven, maximum storm surges (in addition to tide levels) associated with the nine storms with H_s > 5 m ranged from 0.13 to 0.96 m, and for the seven storms at Godrevy the

storm surge levels were 0.19 to 1.19 m. Three of the storms at Porthleven coincided with spring high tide with two of the storm surges exceeding 0.4 m; these storms lasted 4, 16 and 24 hours and were characterized by a maximum H_s of 5, 10.3 and 7 m, respectively. Two of the storms at Godrevy coincided with a spring high tide with a storm surge of 0.53 and 0.9 m; these two storms lasted four and three hours with a maximum H_s of 5.4 and 5 m, respectively. Table II identifies the mean high water neaps (MHWN) and mean high water springs (MHWS) tide levels along with associated storm surges. MHWS occurs at a higher level at Godrevy compared to Porthleven (3.2 m ODN as opposed to 2.5 m ODN). In addition to this, the storm surge levels associated with the 5% exceedance wave events, averaged 0.37 m at Porthleven and 0.5 m at Godrevy.
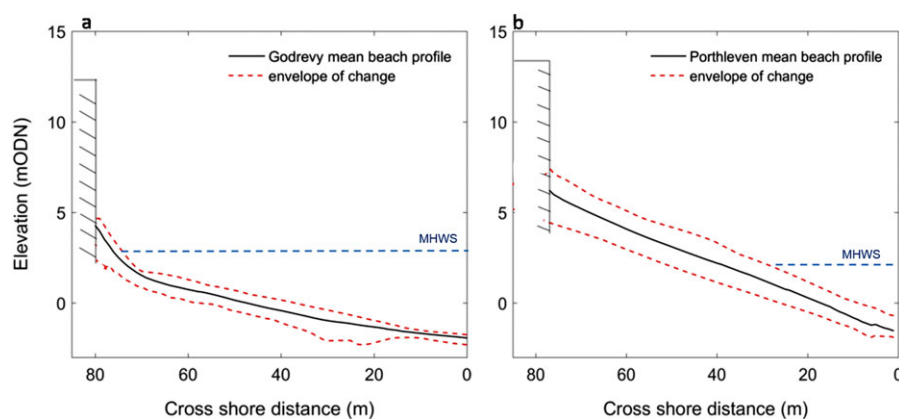
Rainfall totals

Not surprisingly, the wettest periods at both sites correspond with the most energetic wave conditions. The greatest total rainfall values were recorded from October 2013 to February 2014 (> 200 mm) at both sites. The annual variability of rainfall suggests little difference in seasonal rainfall between the two coastlines, but total rainfall suggests the north coast is generally

Table II. Significant wave height (H_s), storm duration and corresponding peak measured surge and surge + tidal elevation [maximum water level (WL)] of events exceeding 5 m H_s, measured on the north (Godrevy) and the south (Porthleven) coasts

	Porthleven				Godrevy				
Storm event	Duration (hours)	Maximum surge	Maximum H_s	Maximum WL (m ODN)	Duration (hours)	Maximum surge	Maximum H_s	Maximum WL (m ODN)	Tidal stage
23–24 December 2013	32	0.75	8.42	2.85	—	—	—	—	S–N
27 December 2013	6	0.44	7.14	2.11	3	0.67	5.0	1.78	N
3–4 January 2014	24	0.47	7	3.59	—	—	—	—	S
6–7 January 2014	29	0.47	7.4	2.5	—	—	—	—	S–N
1 February 2014	4	0.13	5	3.27	4	0.53	5.4	3.37	S (H)
3–5 February 2014	48	0.86	7.7	3.44	3	0.42	5	0.8	S–N
8 February 2014	7	0.54	5	2.06	24	1.19	5.6	2.01	N
12 February 2014	3	0.6	5.1	1.87	7	1.07	5.3	2.3	N–S (H)
14–15 February 2014	16	0.96	10.3	3.51	3	0.9	5	1.4	S
28 February 2014	—	—	—	—	8	0.19	5.1	3.04	N–S (H)
5% exceedance H_s (m)		8.0				5.5			
Average T_p for winter period (seconds)		17				15			
Average surge for winter (m)		0.37				0.50			
MHWS (m ODN)		2.5				3.2			
MHWN (m ODN)		1.3				1.5			

Note: Some of the events occurred on days between springs and neaps. S: spring tide, N; neap tide, H = around high tide (for shorter storms). To represent the average winter conditions, the 5% exceedance H_s, average winter peak wave period (T_p), average winter storm surge are presented, along with the mean high water springs (MHWS) and mean high water neaps (MHWN) levels.

Figure 5. Mean beach cross-shore profiles for (a) Godrevy and (b) Porthleven for the year July 2013–July 2014. The envelope of change is defined by the range between the maximum and minimum beach levels recorded. [Colour figure can be viewed at wileyonlinelibrary.com]

wetter than the south. Over the survey period, Godrevy experienced a total rainfall of 1332 mm with an average monthly rainfall of 102 mm (s.d. = 62 mm), while Porthleven received a total rainfall of 1055 mm with a monthly mean of 82 mm (s. d. = 46 mm). Over the winter period, Godrevy experienced more total rainfall (610 mm) compared to Porthleven (441 mm).

Beach morphology

Both beaches are subject to substantial morphological changes from one survey to the next, both cross-shore and along-shore. In order to understand the dissipation of wave energy prior to reaching the cliff, here we focus on the cross-shore changes to the beach and, in particular, the variability of beach slope and the elevation of the beach at the toe of the cliff (referred to as the b–c junction). The slope of the beach at Godrevy remained around 0.02 (s.d. = 0.005) throughout the year; yet, the elevation of the b–c junction varied by up to 2.2 m, between 2.5 and 4.7 m ODN (Figure 5a).

Porthleven beach is much steeper with a mean slope of 0.17 (s.d. = 0.03) and the elevation of the beach also fluctuated by up to 2–2.5 m across the whole beach in the cross-shore and along-shore (Figure 5). The b–c junction fluctuated between 4.4 and 7 m ODN throughout the year with the lowest elevation and maximum cliff-toe exposure during the winter months (December 2013–March 2014). The stormy conditions in February led to considerable changes in the b–c junction elevation of ±1.5 m over a 12-hour period. The envelope of change is defined by the range between the maximum and minimum levels measured over the year (Figure 5). Relative to the tidal water level, the mean elevation of the b–c junction at Porthleven (~3 m above MHWS) is much higher than at Godrevy (~1 m above MHWS).

Cliff volume changes

From July 2013 to July 2014, the cliffs at Porthleven experienced more than twice the erosion observed at Godrevy, with a total

Table 3. Net cliff erosion volumes for Godrevy and Porthleven from July 2013 – July 2014 (annual retreat rate assumes a 10 m cliff height). Monthly periods are from mid-to-mid month, due to surveys being carried out during spring tide

Survey period 2013 – 2014	Godrevy erosion (m^3)	Porthleven erosion (m^3)
Jul – Aug 2013	27	4
Aug – Sep 2013		1
Sep – Oct 2013	51 (2 months)	3
Oct – Nov 2013	88	35
Nov – Dec 2013	54	
Dec 2013 – Jan 2014	499	1184 (2 months)
Jan – Feb 2014	629	1958
Feb – Mar 2014	148	140
Mar – Apr 2014	28	10
Apr – May 2014	20	18
May – Jun 2014	8	6
Jun – Jul 2014	30	4
Total	**1582**	**3363**
Total upper cliff (head deposit)	*1196 (76%)*	*1739 (52%)*
Total lower cliff (basal layer)	*386 (24%)*	*1624 (48%)*
Mean	144	306
Standard deviation	213	650
Equivalent annual cliff retreat rate	0.5 m yr^{-1}	1.1 m yr^{-1}

volumetric cliff loss of 3633 m^3 compared with 1582 m^3 (Table III). Normalized according to the length of the cliff face (~300 m at each site), this equates to an annual volume loss of 11 m^3 per metre length of cliff at Porthleven and 5.3 m^3 per metre length of cliff at Godrevy. The average cliff height above the beach at Godrevy and Porthleven is 8–15 m and 8–12 m above the beach, respectively (varying according to beach elevation). Assuming an average cliff height of 10 m for both sites, this equates to an equivalent cliff retreat rate of 1.1 m yr^{-1} at Porthleven and 0.5 m yr^{-1} at Godrevy. Significantly less cliff erosion during the spring/summer months (May–September 2013) was recorded, but small-scale changes were detected. Godrevy appeared more susceptible to erosion during the summer (monthly cliff erosion losses of 8 to 30 m^3) than Porthleven (monthly losses of 1 to 18 m^3). At both sites, the erosion volumes were greatest in the winter 2013–2014, with the largest losses measured from December 2013 to March 2014.

Figure 6 indicates the spatial variability in the annual cliff erosion at each site. At Godrevy, the majority of failure (76%) over the one-year survey period occurred within the upper unit of head deposit with the remaining failure (24%) taking place in the basal layer (Table III). The boundary between the two units lies at the very top of the cliff towards the south (Figure 6a) and falls almost to beach level at the northern extent of the cliffs. In this northern region, where the cliff profile is almost entirely
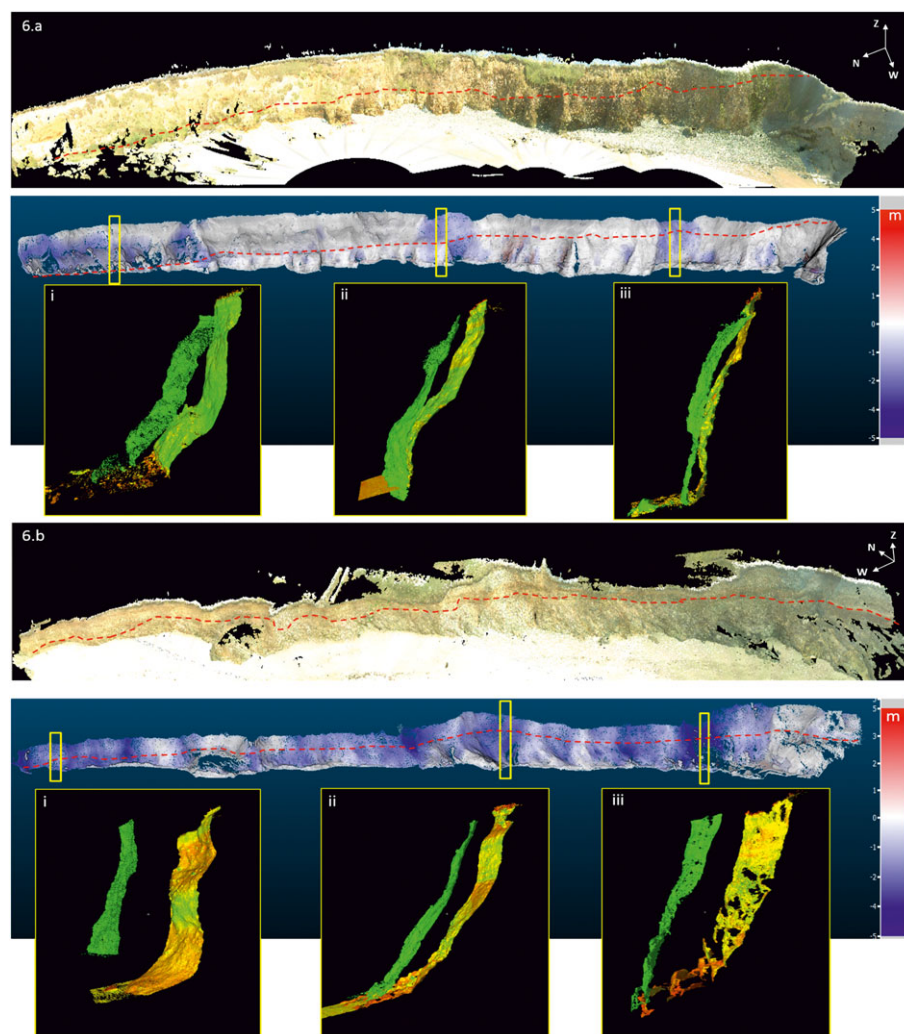

Figure 6. Point cloud of (a) Godrevy and (b) Porthleven cliff face in July 2013 (upper) and annual point cloud comparison plot for July 2013 to July 2014 (lower), with colour bar scale ranging from blue (−5 m) to red (5 m). Dotted red line indicates the boundary between underlying basal layer of Mylor slates and overlying, less resistant quaternary head deposit. (i–iii) Three dimensional (3D) sections through the cliff at three locations where the majority of failure has occurred. Initial surface (July 2013) is depicted in brighter green, superimposed over the later scan (July 2014, yellow-green). [Colour figure can be viewed at wileyonlinelibrary.com]

comprised of head deposit, erosion of the entire cliff-face occurred via rotational sliding, leading to a cliff-normal retreat of 2.3 m (Figure 6ai). Failure in the central section of the cliff (Figure 6aii) occurred via 'slope-over-wall' failure where superficial material has been removed above the underlying basal layer by 2 m. Toward the southern end of the cliffs, erosion is apparent in both the upper unit and the basal layer by 1 m. Cliff erosion across these three sections took place, for the most part, during the winter months (December 2013–March 2014). The erosional volumes during the other months do not reflect the occurrence of any major failures, and are likely to have resulted from a gradual loss of material from the cliff-face.

At Porthleven, the annual difference plot indicates failure occurred relatively evenly along the cliff section (Figure 6b). In both the along-shore and the vertical profile, erosion was detected in the upper unit (52% of the annual retreat) and the lower basal layer (48% of the annual retreat) (Figure 6b; Table III). The boundary between the two units at Porthleven is about half way up the face of the cliff and remains roughly at this level along the entire cliff section. The failure mechanisms are difficult to determine from the annual difference plots as there was no remaining material (i.e. talus deposit) present to indicate rotational sliding or slope-over-wall failure. The entire cliff elevation has retreated almost homogeneously alongshore. Much like Godrevy, the majority of failure at Porthleven occurred during the winter months from December 2013 to March 2014, in both the lower basal layer and in the upper unit. In a two-week period (2–22 February 2014) an overall volume of 1770 m³ was lost over almost the entire cliff elevation across the whole cliff-face. Further failure of the upper unit from overhanging material occurred towards the southern end of the cliffs during the month following this particularly active period.

Wave power – XBeach-G numerical modelling

To collect field measurements of wave conditions to the cliff during storm conditions is very challenging; therefore the numerical model XBeach-G was used to determine the role of the b–c junction elevation and beach slope in modulating the amount of wave energy reaching the cliff under different wave and water level conditions. To account for the highly variable nature of the beach at both sites, three different beach–cliff morphology *scenarios* were considered, representing the average beach slopes (Godrevy: tanβ = 0.02; Porthleven: tanβ = 0.17) and the mean, minimum and maximum b–c junction elevations measured during the survey period (Figure 7).

Table 4. Wave and water levels used to force the XBeach-G model. Average and *maximum* (5% exceedance) wave conditions are taken from the corresponding wave buoy data (see Table 2), Surge levels represent the *mean* surge recorded during the storm periods (Table2). Water levels and b-c junction elevations are presented in m relative to ODN

	Porthleven	Godrevy
Average winter conditions		
H_s (m)	1.8	1.8
T_P (s)	11	12
Maximum **winter conditions**		
0.5 % H_s (m)	8	5.5
T_P (s)	17	15
MHWS	2.5	3.2
MHWS + mean storm surge	2.87	3.7
MHWN	1.3	1.5
MHWN + mean storm surge	1.67	2
Minimum b-c junction	4.4	2.5
Mean b-c junction	6.2	4.3
Maximum b-c junction	7	4.7

Two different wave conditions were used based on the measured inshore wave conditions (Figure 4): average winter conditions over the 2013–2014 winter storm period (H_s = 1.8 m and T_p = 12 seconds for Godrevy; H_s = 1.8 m and T_p = 11 seconds for Porthleven) and to replicate the energetic winter storm conditions over this period, the 5% exceedance H_s and average associated wave period was used (H_s = 5.5 m and T_p = 15 seconds for Godrevy; H_s = 8 m and T_p = 17 seconds for Porthleven). To incorporate tidal elevations and surge effects into the modelling, the measured water levels during the storm periods were replicated at each site (Tables II and IV). MHWS and MHWN lie at 3.2 m and 1.5 m ODN, respectively, at Godrevy and 2.5 m and 1.3 m ODN at Porthleven. Measured water levels (tide plus surge) during the winter 2013–2014 ranged from 0.8 m to 3.4 m, with a mean surge level of 0.5 m at Godrevy and from 1.87 m to 3.6 m, with a mean surge of 0.37 m at Porthleven. To account for this variability in tide and surge elevation over the winter period and replicate the average energetic conditions over the winter as opposed to the absolute short-term peaks in energy four different water level scenarios were selected: MHWS, MHWS plus the average surge, MHWN and MHWN plus the average surge level (Table IV).
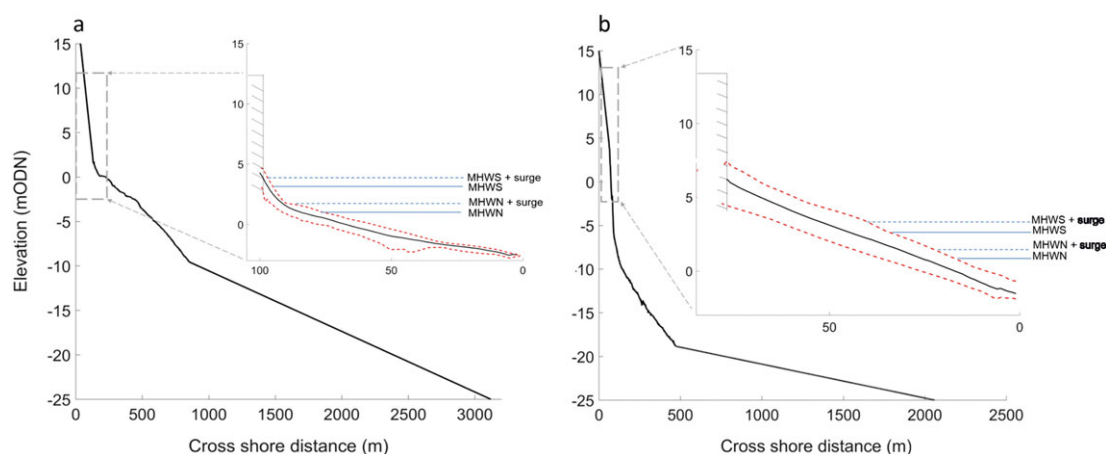

Figure 7. Beach and bathymetric profiles for XBeach-G modelling for (a) Godrevy and (b) Porthleven. Inset illustrates the minimum, mean and maximum beach profiles and beach–cliff junctions and simulated tidal elevations. [Colour figure can be viewed at wileyonlinelibrary.com]
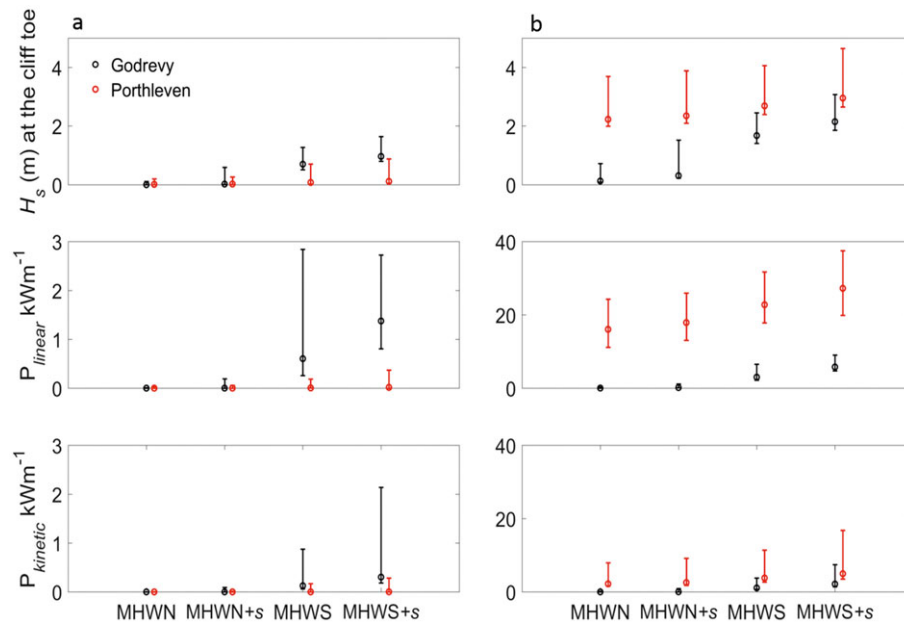
Figure 8. XBeach-G model output of H_s at the toe of the cliff under varying water level conditions (MHWN and MHWS plus mean surge level) for (a) average winter conditions (left panel) and (b) maximum conditions (5% exceedance H_s) over the winter period (right panel). Wave power (lower four panels) at the beach–cliff (b–c) junction is calculated using two different methods to give the energy using linear wave theory (P_{lin}) (central panels) and the kinetic energy (P_{kin}) (lower panels) as per Equations (1) and (2). The upper (lower) limit of the error bar represents the minimum (maximum) b–c junction elevation, whereas the circles represent the mean b–c junction elevation. [Colour figure can be viewed at wileyonlinelibrary.com]

The slope of the beach and the b–c junction elevation with respect to MHWS suggests that, on average, the cliffs at Godrevy are subject to more frequent inundation than those at Porthleven (Figure 5). Ignoring wave action, at Godrevy the cliff-toe is inundated during MHWS, whereas at Porthleven virtually no cliff-toe inundation occurs for any of the four water level scenarios (Figure 7). However, it is the exposure of the cliff-toe under extreme wave conditions that is of importance here, and for this model simulations are required. The modelled wave height (H_s) and wave power (P_{linear} and $P_{kinetic}$) at the cliff-toe for the different wave energy, water level and b–c junction scenarios for the two study sites are presented in Figure 8.

Encouragingly, the amount of wave energy reaching the cliff according to the two different methods (P_{linear} and $P_{kinetic}$) (Equations (1) and (2)) yields relatively comparable results for the different b–c junctions and water levels, except for maximum wave conditions at Porthleven where P_{linear} exceeds $P_{kinetic}$ under all b–c junction and tide scenarios. Focusing first on the average winter wave conditions (Figure 8a – left panels), the base of the cliff at Godrevy experiences more energetic conditions (H_s) than Porthleven during spring tide conditions both with and without a storm surge and comparable conditions during a neap high tide. Unsurprisingly, very little energy is delivered to either cliff during a neap high tide ($H_s < 1$ m; P_{linear} and $P_{kinetic} < 0.05$ kW m^{-1}). The most energetic winter average conditions at the base of both cliffs occur during spring high tide (with and without a storm surge) with a low b–c junction, characterized by typical values of $H_s = 0.5$–1 m and $P_{linear} = 2$–2.8 kW m^{-1}. A different picture emerges during peak (5% exceedance H_s) storm conditions (Figure 8b – right panels) when the modelled results show that Porthleven receives considerably larger H_s values at the cliff-toe and more wave energy under all tide and b–c junction scenarios. This is to be expected as the peak offshore H_s was 8 m at Porthleven compared to 5.5 m Godrevy. It is noteworthy to mention that XBeach-G predicted > 4 m high waves (swashes) directly impacting the cliff at Porthleven under peak storm conditions with a low b–c junction and during spring high tide (upper panel of Figure 8b). This

is in agreement with field observations at this site (supplementary video clip in Earlie *et al.*, 2015).

Comparing the wave power at the toe of the cliff for winter-average wave conditions with maximum storm wave conditions, under a minimum b–c junction scenario, P_{linear} at Godrevy increases from 0 to 2.9 to 0.2–9 kW m^{-1} ($P_{kinetic}$ increases from 0 to 2.1 to 0.02–7 kW m^{-1}) and P_{linear} at Porthleven increases from 0.03–0.4 to 24–39 kW m^{-1} ($P_{kinetic}$ increases from 0.01–0.4 to 8–19 kW m^{-1}). For the maximum storm wave conditions, wave power values calculated using the first approximation according to linear wave theory at the cliff-toe at Porthleven are more than four times that at Godrevy, and this difference is larger than that could be expected on the basis of the differences in the offshore wave forcing (where the 5% exceedance H_s at Porthleven is only 1.45 times greater than at Godrevy, which should result in a factor 2 increase in resultant wave energy). This suggests that the higher wave energy at the toe of the cliff at Porthleven cannot solely be attributed to the more energetic wave conditions at this site.

Discussion

Figure 9 summarizes the monthly cliff erosion rates and the various forcing and controlling factors. Wave and weather conditions over the one-year study period were consistent across the two study sites with more energetic waves and wetter conditions in the winter compared with the summer. It is evident, however, that during the winter period, Godrevy experienced more rainfall than Porthleven. In terms of cliff exposure/inundation, the beach at Porthleven provided more protection on average to cliff than at Godrevy with the mean b–c junction > 2.5 m above MHWS compared to ~1 m. The difference in erosion volumes for the year (Porthleven = 3363 m^3, Godrevy = 1582 m^3), cliff failure patterns and timings tend to suggest a disparity in assailing and/or resisting forces between the two sites (Figure 9).
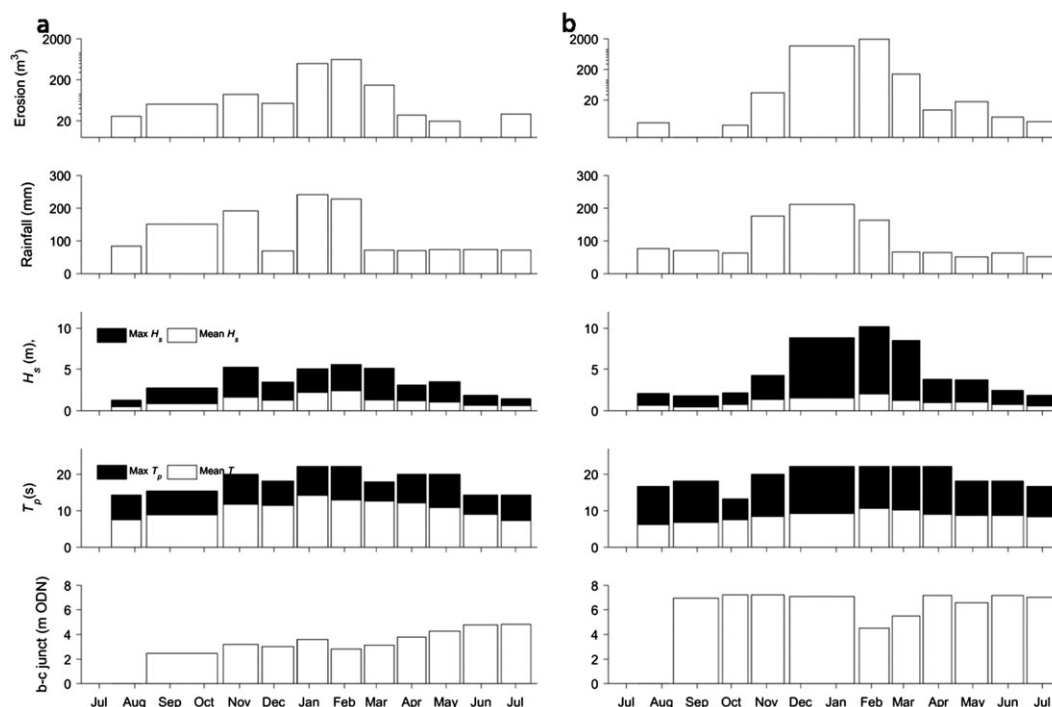
Figure 9.   Summary of results from the monthly surveys, showing, from top to bottom: cliff face erosion volume, rainfall, maximum and mean monthly significant wave heights (H_s) and wave periods (T_p), and beach–cliff (b-c) junction elevation. Left panel (a) for Godrevy and right panels (b) for Porthleven. Length of survey period is represented by the width of the bars.

Two key factors that are thought to contribute to the difference in cliff erosion rates between the two sites are the difference between the extreme winter wave conditions at each site and the morphology (slope of the upper shoreface and b–c junction of the beach) in modifying wave energy delivery (as well as protection) to the cliffs. Recent studies have also highlighted the influence of extreme wave conditions on the erosion of sea-cliffs (Young *et al.*, 2013; Brain *et al.*, 2014; Earlie *et al.*, 2015; Vann Jones *et al.*, 2015). The inshore wave climate over the winter was much more energetic along the south coast compared to the north, with the south coast not only experiencing a greater number of storms exceeding 5 m H_s over that winter, but also a greater number of storms coinciding with a spring high tide (three at Porthleven; two at Godrevy), with longer durations (four to 24 hours and three to four hours) and greater significant wave heights [8 m and 5.5 m (5 % exceedance H_s)]. Therefore, one of the reasons for the greater magnitude of cliff erosion at Porthleven compared to Godrevy is likely to be have been influenced by the cumulative effect of a more energetic inshore wave climate over that particular winter.

Previous studies have emphasized how the volume of the beach above rock platforms and, hence, the position of the still water line relative to the cliff-toe is important in dictating cliff-toe inundation, wave attack and subsequent long-term platform down wearing and cliff erosion (Ruggerio *et al.*, 2001, 2004; Walkden and Hall, 2005, 2011; Lee, 2008; Trenhaile, 2009, 2016). This is apparent in the spring/summer months, when regular tidal inundation of the cliff-toe was inhibited by the beach at Porthleven, although not at Godrevy due to the lower beach elevation. As a consequence, modelled wave energy delivery to the cliff at Porthleven only occurs during a spring high tide and a minimum b–c junction (Figure 8a) and erosion values over the spring/summer were considerably greater at Godrevy than Porthleven (Table III).

During the winter, however, when wave energy is much higher and the erosion of the cliffs was much greater at Porthleven than Godrevy, the interaction between the storm waves and the beach tends, through transformation of waves across the upper shoreface and wave run-up, to play a more important role than still water levels in controlling wave energy delivery to the cliffs. This is evident in the amplification of wave energy seen at the different beach profiles in the XBeach-G modelling. On steeper beaches, wave break closer to the cliffs (Walkden and Hall, 2005; Trenhaile 2005, 2009, 2016), with little time and distance to dissipate energy after wave breaking, resulting in higher run-up heights (Stockdon *et al.*, 2006; Poate *et al.*, 2016). This is demonstrated in Figure 8, which shows that, under extreme storm conditions (5.5 m for Godrevy and 8 m at Porthleven), the wave energy experienced at the toe of the cliff at Porthleven is up to 4.2 times greater (when considering the first approximation, P_{linear}, and 2.7 times greater with $P_{kinetic}$) than at Godrevy, whereas the maximum inshore wave height at Porthleven is only 1.45 times that at Godrevy. The higher levels of wave energy reaching the cliff-toe at Porthleven is, therefore, at least partly, attributed to the larger wave run-up at this location due to the steeper beach gradient.

The influence beach slope and offshore bathymetry have on wave energy delivery to the cliffs is further illustrated and emphasized with additional XBeach-G model simulations. The purpose of this was to explore, hypothetically, the influence the offshore slope and beach profile have on the resultant wave power (P_{linear}) reaching the cliffs at both sites under the same forcing conditions (Figure 10).

Using the same H_s and T_p scenarios and the maximum wave conditions measured at both of the beaches (H_s = 5.5 m, T_p = 15 seconds; H_s = 8 m, T_p = 17 seconds), the wave power measured along the coastal slope and beach profile varied quite dramatically between the sites (Figure 10). Increasing the wave conditions from H_s = 5.5 m, T_p = 15 seconds to H_s = 8 m, T_p 17 seconds leads to an increase in wave energy of a factor 2 at the cliff face at Porthleven, compared to a factor 1.3 increase at Godrevy, implying the difference in beach slope and the wave energy dissipation across the shore face prior to cliff impact is a contributing factor to the disparity between wave power
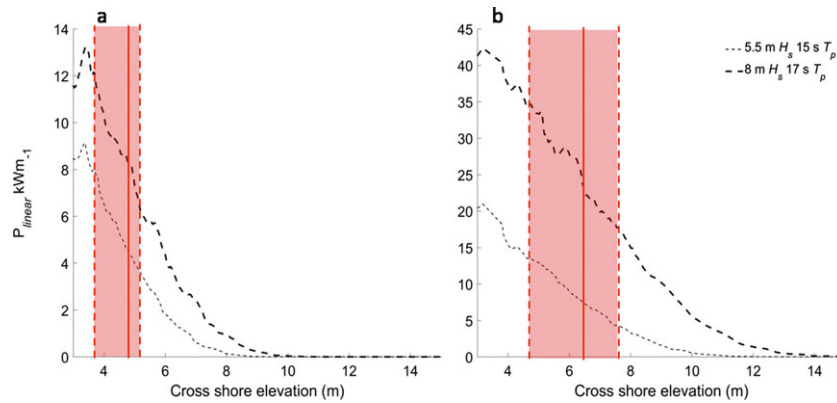
Figure 10. XBeach-G model simulations of P_{linear} for Godrevy (a) and Porthleven (b) for the maximum wave conditions measured at both the beaches under maximum water levels (MHWS plus mean surge level). The wave power (Equation (1)) at the mean beach–cliff (b–c) junction (solid red lines) and the minimum and maximum b–c junction (dotted red lines) were extracted along the cross-shore profile in the model. [Colour figure can be viewed at wileyonlinelibrary.com]

experienced at the cliffs. Considering this maximum wave condition (H_s = 8 m and T_p = 17 seconds) the wave power measured 12 kW m^{-1} about 10 m from the face of the cliff at Godrevy and at Porthleven, with the same wave conditions, the wave power reached 42 kW m^{-1} 5–10 m from the cliff face. These model simulations demonstrate that if Godrevy would have experienced the Porthleven maximum wave conditions, or if Porthleven would have experienced the Godrevy maximum wave conditions, in both cases the energy at the base of the cliff at Porthleven would still have been a factor 3.5 larger than at Godrevy.

Modelling the wave–cliff interaction under these different forcing scenarios and beach configurations provides valuable insight into some of the key factors that influence cliff erosion rates and provides an explanation for the differing erosion rates at the two sites. The wave energy delivery to the cliff-face, and therefore the degree of wave–cliff impact and cliff erosion volumes, is governed not only by the incident wave conditions and the water levels relative to the elevation of the b–c junction, but also to differences in the morphology of the beach fronting the cliffs. Specifically, the gradient of the upper shoreface and the morphodynamic state (reflective versus dissipative) directly influences the transformation of waves across the beach, wave dissipation and the delivery of wave energy to the cliff-face, particularly under extreme wave conditions.

Geomorphic context

The results of this study have provided insight into the short-term episodic processes that are averaged out in long-term methods of deriving erosion rates. It is not appropriate to

compare these short-term rates of retreat with rates derived over longer periods of time; however, comparing the rates of cliff erosion derived under different timescales places the significance of these extreme events into context (Moore and Griggs, 2002). It is important to note, however, that this particular winter was the most energetic (in terms of wave climate), the southwest UK has seen in at least 60 years (Masselink et al., 2016).

The erosion rates at Godrevy and Porthleven calculated over the one-year survey period are 0.5 and 1.1 m yr^{-1}, respectively, and these are one-order of magnitude greater than the long-term rates established using LiDAR for the period 2007–2008 to 2010–2011 (Earlie et al., 2014), and even larger in comparison to cliff erosion rates derived with historic map analysis representing 50–100 years (Orford et al., 2002) (Figure 11). The cliff erosion during 2013–2014 primarily occurred during the most energetic months of this period and the equivalent annual erosion rate at Porthleven and Godrevy during the January–February 2014 period was 3.9 and 1.3 m yr^{-1}, respectively.

The results imply that two important parameters need to be considered when investigating monthly/seasonal changes to the cliffs. Firstly, the morphology of the beach fronting the cliffs (i.e. the slope of the beach, the volume of the beach and the elevation of the beach at the toe of the cliffs), and secondly the influence these parameters have on the resultant nearshore hydrodynamics, particularly wave breaking patterns and surf zone dissipation under extreme storm conditions. It is these short-term processes that tend to be highly influential in determining the episodic nature of failure, a factor that will be prudent to consider as high-magnitude, low-frequency events could become more frequent in the future with the risk of
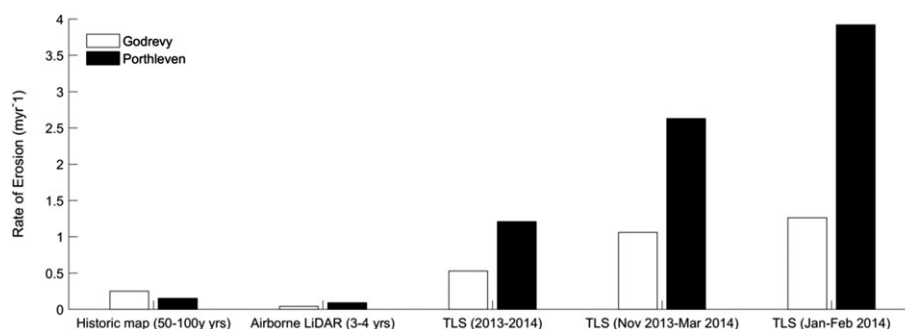

Figure 11. Erosion rates for Porthleven and Godrevy. Historic map rates from (Orford et al., 2002) Airborne LiDAR rates from Earlie et al. (2013, 2014), terrestrial laser scanning (TLS) rates from monthly scans over the one-year period and the contribution of the winter erosion volumes (December–March) and storm period (January–February) to the total erosion from the year 2013–2014. These values are calculated to an equivalent per year rate.

increase storminess associated with climate change (Cowell, 2006; Barros *et al.*, 2014; Haigh *et al.*, 2016).

Conclusions

Monthly TLS surveys of coastal cliffs at two particularly vulnerable sites in southwest England were conducted over a one-year period, which included the most energetic winter (2013–2014) since 1948. One of the cliff sites was fronted by a gently-sloping dissipative beach with a relatively low b–c junction (around MSL), whereas the other site was fronted by a steep reflective beach with a relatively high b–c junction (around MHWS). Both sites experienced extreme wave conditions, but maximum wave energy levels at the reflective site (H_s = 8 m) were higher than at the dissipative site (H_s = 5.5 m); average winter wave conditions were similar (H_s < 2 m). At both sites, the 8–15 m cliffs are characterized by fractured meta-sedimentary rocks capped with less resistant head deposits.

A strong seasonal variability in cliff erosion was apparent with more than 90% of the cliff volumetric losses occurring during the winter months (December–March). Erosion volumes over the one-year period were found to be twice as great at the cliff site fronted by the reflective beach (1.1 m yr^{-1}) compared with at a dissipative beach (0.5 m yr^{-1}). These cliff erosion rates are a factor three to five times larger than the long-term average, testifying to the importance of extreme storm conditions to long-term cliff evolution.

The larger erosion rate at the reflective site is partly attributed to the more energetic inshore wave conditions at this site; however, a very significant role is also played by the beach morphology through its influence on the delivery of wave energy to the base of the cliff. This role was explored using the numerical model XBeach-G forced with local conditions (waves, tides and beach morphology).

The numerical model results demonstrate that under relatively modest wave conditions (H_s < 2 m), the elevation of the b–c junction relative to the tide level is the most important factor in controlling the delivery of wave energy at its base (favouring more frequent inundation at the dissipative site). However, under storm wave conditions, the beach gradient, through its control on wave run-up, is the more important factor (favouring more frequent inundation at the reflective site), especially under extreme wave conditions. Simulating the maximum wave conditions experienced at both sites, the amount of wave energy reaching the base of the cliff fronted by the reflective beach was more than four times higher than at the dissipative site. Simulating the same maximum wave conditions at both sites highlighted that even under the same forcing conditions, the cliffs fronted by a reflective beach were subject to waves 3.5 times more powerful than the dissipative beach.

The results captured using a combination of remote sensing (TLS) and *in situ* instrumentation (pressure sensors, wave buoys), accompanied by numerical modelling, show that site specific-investigations of extreme storms on coastal cliffs and the interaction of waves with the beach and cliffs are not only obtainable, but essential in understanding how these episodic extreme events affect cliffed coastlines in a longer term context.

References

Abellan A, Calvet J, Vilaplana JM, Blanchard J. 2010. Detection and spatial prediction of rock falls by means of terrestrial laser scanner monitoring. *Geomorphology* **119**: 162–171.

Abellan A, Vilaplana JM, Calvet D, Garcia-Selles D, Asensio E. 2011. Rockfall monitoring by Terrestrial Laser Scanning – case study of the basaltic rock face at Castellfollit de la Roca (Catalonia, Spain). *Natural Hazards Earth System Science* **11**: 829–841.

Alexander AC, Shail RK. 1996. Late-to post-Variscan structures on the coast between Penzance and Pentewan, south Cornwall. *Proceedings of the Ussher Society* **9**: 72–78.

Austin MJ, Scott TM, Russell PE, Masselink G. 2012. Rip current prediction: development, validation, and evaluation of an operational tool. *Journal of Coastal Research* **29**(2): 283–300.

Barros VR, Field CB, Dokke DJ, Mastrandrea MD, Mach KJ, Bilir TE, Chatterjee M, Ebi KL, Estrada YO, Genova RC, Girma B. 2014. *Climate Change 2014: Impacts, Adaptation, and Vulnerability. Part B: Regional Aspects. Contribution of Working Group II to the Fifth Assessment Report of the Intergovernmental Panel on Climate Change (IPCC)*. IPCC: Geneva.

Bird ECF. 1998. *The Coasts of Cornwall: Scenery and Geology with an Excursion Guide*. Alexander Associates: London.

Brain JM, Rosser NJ, Norman EC, Petley DN. 2014. Are microseismic ground displacements a significant geomorphic agent? *Geomorphology* **207**: 161–173.

Brodu N, Lague D. 2012. 3D terrestrial LiDAR data classification of complex natural scenes using a multi-scale dimensionality criterion: applications in geomorphology. *ISPRS Journal of Photogrammetry and Remote Sensing* **68**: 121–134.

Carpenter NE, Dickson ME, Walkden MJA, Nicholls RJ, Powrie W. 2014. Effects of varied lithology on soft-cliff recession rates. *Marine Geology* **354**: 40–52.

Channel Coastal Observatory (CCO). 2015. Map Viewer and Data Catalogue. http://www.channelcoast.org/data_management/online_data_catalogue/ [February 2015].

Cowell PJ, Thom BG, Jones RA, Everts CH, Simanovic D. 2006. Management of uncertainty in predicting climate-change impacts on beaches. *Journal of Coastal Research* **7**: 53–84.

Dewez TJB, Rohmer J, Regard V, Cnudde C. 2013. Probabilistic coastal cliff collapse hazard from repeated terrestrial laser surveys: case study from Mesnil Val (Normandy, northern France). In *Proceedings 12th International Coastal Symposium* (Plymouth, UK), Conley DC, Masselink G, Russell PE, O'Hare TJ (eds). *Journal of Coastal Research* **65**(Special Issue): 702–707.

Dickson M, Walkden MJ, Hall J. 2007. Systematic impacts of climate change on an eroding coastal region over the twenty-first century. *Climatic Change* **84**: 141–166.

Duperret A, Taibi S, Mortimore RN, Daigneault M. 2005. Effect of groundwater and sea weathering cycles on the strength of chalk rock from unstable coastal cliffs of NW France. *Engineering Geology* **78**: 321–343.

Earlie CS. 2015. Field Observations of Wave Induced Coastal Cliff Erosion; Cornwall, UK, PhD Thesis. School of Marine Science and Engineering, Plymouth University.

Earlie CS, Masselink G, Russell PA, Shail RK. 2013. Sensitivity analysis of the methodology for quantifying cliff erosion using airborne LiDAR - examples from Cornwall, UK. In *Proceedings 12th International Coastal Symposium* (Plymouth, England), Conley DC, Masselink G, Russell PE, O'Hare TJ (eds). *Journal of Coastal Research* **65**(Special Issue): 470–475, ISSN 0749-0208.

Earlie CS, Masselink G, Russell PE, Shail RK. 2014. Application of airborne LiDAR to investigate rates of recession in rocky coast environments. *Journal of Coastal Conservation: Planning and Management* **19**(6): 831–845. https://doi.org/10.1007/s11852-014-0341.

Earlie CS, Young AP, Masselink G, Russell PE. 2015. Coastal cliff ground motions and response to extreme storm waves. *Geophysical Research Letters* **42**: 847–854. https://doi.org/10.1002/2014GL062534.

Emery KO, Kuhn GG. 1982. Sea cliffs: their processes, profiles and classification. *Geological Society of America Bulletin* **93**: 644–654.

Haigh ID, Wadley MP, Wahl T, Ozsoy O, Nicholls RJ, Brown JM, Horsburgh K, Gouldby B. 2016. Spatial and temporal analysis of

extreme sea level and storm surge events around the coastline of the UK. *Nature: Scientific Data* **3**: 160107. https://doi.org/10.1038/sdata.2016.107.

Komar PD. 1998. *Beach Processes and Sedimentation*, 2nd edn. Prentice-Hall: Upper Saddle River, NJ.

Kuhn D, Prufer S. 2014. Coastal cliff monitoring and analysis of mass wasting processes with the application of terrestrial laser scanning: a case study of Rugen. *Germany, Geomorphology* **213**: 153–165.

Lague D, Brodu N, Leroux J. 2013. Accurate 3D comparison of complex topography with terrestrial laser scanner: application to the Rangitikei canyon (NZ). *ISPRS Journal of Photogrammetry and Remote Sensing* **82**: 10–26. https://doi.org/10.1016/j.isprsjprs.2013.04.00.

Lee EM. 2002. *Soft Cliffs: Prediction of Recession Rates and Erosion Control Techniques*. DEFRA/Environment Agency, Flood and Coastal Defence R&D Programme, DEFRA Flood and Management Division: London.

Lee EM. 2008. Coastal cliff behaviour: observations on the relationship between beach levels and recession rates. *Geomorphology* **101**(4): 558–571.

Leica. 2015. Leica Cyclone, 3D Point Cloud Processing Software (version 8.1) [Software]. http://hds.leica-geosystems.com/en/Leica-Cyclone_6515.htm

Leveridge BE, Shail RK. 2011. The Gramscatho Basin, south Cornwall, UK: Devonian active margin successions. *Proceedings of the Geologists' Association* **122**: 568–615.

Lim M, Rosser NJ, Petley DN, Keen M. 2011. Quantifying the controls and influence of tide and wave impacts on coastal rock cliff erosion. *Journal of Coastal Research* **27**(1): 46–56.

Limber PW, Murray AB. 2011. Beach and sea cliff dynamics as a driver of rocky coast line evolution and stability. *Geology* **39**: 1149–1152.

Masselink G, Castelle B, Scott T, Dodet G, Suanez S, Jackson D, Floc'h F. 2016. Extreme wave activity during 2013/2014 winter and morphological impacts along the Atlantic coast of Europe. *Geophysical Research Letters* **43**(5): 2135–2143.

Masselink G, Hughes MG. 2003. *Introduction to Coastal Processes and Geomorphology*. Arnold: London.

McCall RT, Masselink G, Poate TG, Roelvink JA, Almeida LP, Davidson M, Russell PE. 2014. Modelling storm hydrodynamics on gravel beaches with XBeach-G. *Coastal Engineering* **91**: 231–250.

Met Office. 2012. South-west England: Climate. [Online] http://www.metoffice.gov.uk/climate/uk/sw/print.html [February 2015].

Moore LJ, Griggs GB. 2002. Long-term cliff retreat and erosion hotspots along the central shores of the Monterey Bay National Marine Sanctuary. *Marine Geology* **181**(1–3): 265–283. https://doi.org/10.1016/S0025-3227(01)00271-7.

Norman EC. 2012. Microseismic Monitoring of the Controls on Coastal Rock Cliff Erosion, PhD Thesis. Department of Geography, Durham University.

Norman EC, Rosser NJ, Brain MJ, Petley DN, Lim M. 2013. Coastal cliff-top ground motions as proxies for environmental processes. *Journal of Geophysical Research – Oceans* **118**: 6807–6823.

National Tidal and Sea Level Facility (NTSLF). 2014. Real time data, UK National Tide Gauge Network [Online] https://www.ntslf.org/ [January 2014].

Orford J, Burgess K, Dyer K, Townend I, Balson P. 2002. 'FUTURECOAST' – The integration of knowledge to assess future coastal evolution at a National scale. *Paper Presented at 28th International Conference on Coastal Engineering*, Cardiff; 3221–3233.

Pethick J. 1984. *An Introduction to Coastal Geomorphology*. Arnold: London.

Poate T, Kingston K, Masselink G, Russell P. 2009. Response of high-energy, macro tidal beaches to seasonal changes in wave conditions: examples from North Cornwall, UK, *Proceedings of the 10th International Coastal Symposium*, Lisbon, Portugal. *Journal of Coastal Research* **56**(Special Issue): 747–751.

Poate T, McCall RT, Masselink G. 2016. A new parameterisation for run-up on gravel beaches. *Coastal Engineering* **117**: 176–190.

Poulton CVL, Lee JR, Hobbs PRN, Jones L, Hall M. 2006. Preliminary investigation into monitoring coastal erosion using terrestrial laser scanning: case study at Happisburgh, Norfolk. *The Bulletin of the Geological Society of Norfolk* **56**: 45–64.

Rohmer J, Dewez T. 2013. On the deviation of extreme sea-cliff instabilities from the power-law frequency-volume distribution: practical implications for coastal management. *Proceedings of the 12th International Coastal Symposium*, Plymouth, England, Conley DC, Masselink G, Russell PE, O'Hare TJ (eds). *Journal of Coastal Research* **65**(Special Isuue): 1698–1703.

Rosser N, Lim M, Petley D, Dunning S, Allison R. 2007. Patterns of precursory rockfall prior to slope failure. *Journal of Geophysical Research – Earth Surface* **112**: F04014. https://doi.org/10.1029/2006JF000642.

Rosser NJ, Petley DN, Lim M, Dunning SA, Allison RJ. 2005. Terrestrial laser scanning for monitoring the process of hard rock coastal cliff erosion. *Quarterly Journal of Engineering Geology and Hydrogeology* **38**(4): 363–375.

Ruggerio P, Holman RA, Beach RA. 2004. Wave run-up on a high-energy dissipative beach. *Journal of Geophysical Research – Oceans* **109**(6). https://doi.org/10.1029/2003JC002160.

Ruggerio P, Komar PD, McDougal WG, Beach RA. 1996. Extreme water levels, wave run-up and coastal erosion. In *Proceedings of the 25th International Conference on Coastal Engineering*. American Society of Civil Engineers: Orlando, FL.

Ruggerio P, Komar PD, McDougal WG, Marra JJ, Beach RA. 2001. Wave run-up, extreme water levels and the erosion of properties backing beaches. *Journal of Coastal Research* **17**(2): 407–419.

Sallenger AH, Jr, Krabill W, Brock J, Swift R, Manizade S, Stockdon H. 2002. Sea-cliff erosion as a function of beach changes and extreme wave run-up during the 1997–1998 El Nino. *Marine Geology* **187**: 279–297.

Scott T, Masselink G, Russell P. 2011. Morphodynamic characteristics and classification of beaches in England and Wales. *Marine Geology* **286**: 1–20.

Scott TM. 2012. UKBSAM: Database of Physical Hazards at Designated UK Bathing Beaches. RNLI risk assessment database.

Shail R, Coggan J, Stead D. 1998. Coastal land sliding in Cornwall, UK: mechanisms, modelling and implications. *Proceedings of the 8th International Congress of the International Association for Engineering Geology and the Environment*, Vancouver, Canada; 1323–1330.

Shail RK, Coggan JS. 2010. Godrevy Coastal Recession Baseline Survey 2009–2010. Camborne School of Mines, University of Exeter: Exeter.

Shih SM, Komar PD, Tillitson KJ, McDougal WG, Ruggerio P. 1994. Wave run-up and sea-cliff erosion. In *Proceedings of the 24th Coastal Engineering Conference*. American Society of Civil Engineers: Orlando, FL; 2170–2184.

Stockdon HF, Holman RA, Howd PA, Sallenger AH, Jr. 2006. Empirical parameterization of setup, swash and run-up. *Coastal Engineering* **53**: 573–588.

Sunamura T. 1976. Feedback relationship in wave erosion of laboratory rocky coast. *Journal of Geology* **84**: 427–437.

Sunamura T. 1992. *Geomorphology of Rocky Coasts*. John Wiley & Sons: Chichester.

Travelletti J, Malet JP, Delacourt C. 2014. Image-based correlation of laser scanning point cloud time series for landslide monitoring. *International Journal of Applied Earth Observation and Geoinformation* **32**: 1–18.

Trenhaile AS. 1987. *The Geomorphology of Rock Coasts*. Clarendon Press: Oxford.

Trenhaile AS. 2005. Modelling the effect of waves, weathering and beach development on shore platform development. *Earth Surface Processes and Landforms* **30**: 613–634.

Trenhaile AS. 2009. Modelling the erosion of cohesive clay coasts. *Coastal Engineering* **56**: 59–72.

Trenhile AS. 2016. Rocky coasts – their role as depositional environments. *Earth Science Reviews* **159**: 1–13.

UK Hydrographic Office (UKHO). 2016. Products and Services. [Online] http://www.ukho.gov.uk/ProductsandServices/Pages/Home.aspx [November 2016].

Vann Jones EC, Rosser NJ, Brain MJ, Petley DN. 2015. Quantifying the environmental controls on erosion of a hard rock cliff. *Marine Geology* **363**: 230–242.

Walkden MJ, Dickson M. 2008. Equilibrium erosion of soft rock shores with a shallow or absent beach under increased sea level rise. *Marine Geology* **251**: 75–84.

Walkden MJ, Hall JW. 2005. A predictive Mesoscale model of the erosion and profile development of soft rock shores. *Coastal Engineering* **52**: 535–563.

Walkden MJ, Hall JW. 2011. A mesoscale predictive model of the evolution and management of a soft-rock coast. *Journal of Coastal Research* **27**: 529–543.

Wyllie DC, Mah CW. 2004. *Rock Slope Engineering: Civil and Mining*, 4th edn. Spon Press: London.

Young AP, Adams P, O'Reilly WC, Flick RE, Guza RT. 2011. Coastal cliff ground motions from local ocean swell and infragravity waves in southern California. *Journal of Geophysical Research* **116**: C09007. https://doi.org/10.1029/2011jc007175.

Young AP, Ashford SA. 2006. Application of airborne LiDAR for seacliff volumetric change and beach-sediment budget contributions. *Journal of Coastal Research* **22**: 307–318.

Young AP, Guza RT, Adams PN, O'Reilly WC, Flick RE. 2012. Cross-shore decay of cliff top ground motions driven by local ocean swell and infragravity waves. *Journal of Geophysical Research* **117**: C06029. https://doi.org/10.1029/2012JC007908.

Young AP, Guza RT, Dickson ME, O'Reilly WC, Flick RE. 2013. Ground motions on rocky, cliffed, and sandy shorelines generated by ocean waves. *Journal of Geophysical Research – Oceans* **118**: 6590–6602. https://doi.org/10.1002/2013JC008883.

Young AP, Flick RE, O'Reilly WC, Chadwick DB, Crampton WC, Helly JJ. 2014. Estimating cliff retreat in southern California considering sea level rise using a sand balance approach. *Marine Geology* **348**: 15–26. https://doi.org/10.1016/j.margeo.2013.11.007.

Young AP, Guza RT, O'Reilly WC, Burvingt O, Flick RE. 2016. Observations of coastal cliff base waves, sand levels, and cliff top shaking. *Earth Surface Process and Landforms* **41**(11): 1564–1573.